Evaluation of Deceptive Jamming Effect on SAR Based on Visual Consistency

Zhouyang Tang, Chunrui Yu, Yunkai Deng, *Member, IEEE*, Tingzhu Fang, and Huifang Zheng

***Abstract*—In complicated electromagnetic environments, synthetic aperture radar (SAR) can be threatened by various kinds of malicious interference, of which deceptive jamming is the intentional and efficient one. For jamming effect evaluation on SAR images, traditional methods are mostly based on the change of image quality, which are not suitable for evaluating the confusion caused by high-fidelity false targets. In this article, a novel framework to evaluate the effect of deceptive jamming on SAR is proposed based on visual consistency. Three levels of vision, namely detection, recognition, and semantics, are fused for efficient deception evaluation along with the corresponding metrics system. Fully considering the imaging characters of deceptive jamming, specifically designed detection and recognition flows are proposed to quantitatively evaluate the deception. Furthermore, to evaluate whether the generated false targets are with reasonable context, an unprecedent concept, named semantic accuracy, is proposed via considerations of statistical differences compared with that of the background template. Besides, the cases of deceptive jamming with several common nonideal issues are considered when evaluating the effects. Sufficient experiments have proved the practicality and superiority of the proposed evaluation framework under different deceptive jamming with various nonideal factors.**

***Index Terms*—Deceptive jamming effect evaluation, detection and recognition, semantic accuracy, synthetic aperture radar (SAR), visual consistency (VC).**

I. Introduction

SYNTHETIC aperture radar (SAR) is an advanced microwave imaging equipment for Earth observation. Due to the capacity of imaging all weather and all time, SAR has been widely used in civil fields [1]–[3] and military applications [4], [5]. Meanwhile, the research on jamming technology for SAR has been greatly supported and invested [6]–[10], and numerous jamming methods and systems are constantly developed. Deceptive jamming is one of the effective ways due to its 2-D coherence with respect to the SAR signal. Nevertheless, effective evaluation of deceptive jamming effect on SAR is rarely raised, which motivates this article.

An effective method of jamming effect evaluation can not only quantitatively describe the effect of jamming on SAR imaging, but also, in turn, guide the optimization of jamming methods. Existing jamming evaluation methods can be divided into the following three categories, namely information criterion [11]–[20], power criterion [21], and efficiency criterion [22]–[25].

1) *Information criterion:* The information criterion considers the loss of information or the change of image quality after being jammed, which is the most widely used. The cross entropy is considered for jamming effect evaluation in [11], but the principle explanation and experimental setup are relatively rough. In [12], mutual information is clearly deduced and mathematically related to other types of entropy. The physical significance is explained more distinctly, and extensive experiments confirm its high effectiveness. Additionally, for more accurate depiction of information differences, the improved cross entropy further considers the spatial relationship [13]. On the other hand, the information criteria also consider that the change of image quality occurs in a jammed image. The peak sidelobe ratio and the integrated sidelobe ratio are two typical evaluation metrics for point targets [14]. For area targets, Euclidean distance, correlation coefficient, structural similarity index (SSIM), image entropy, and equivalent number of looks (ENL) [15]–[19] are usually employed for the convenience. Moreover, for evaluation results being more consistent with the human visual system, edge strength images are recommended to be obtained first before calculating the correlation coefficient in [16], and textural feature extraction in the weighted wavelet domain is introduced in [20].
2) *Power criterion:* Based on the system parameters of the jammer and SAR, the power criterion considers the effective radiated power required for the jammer to achieve the predetermined jamming effect [21]. Nevertheless, the jamming-to-signal ratio is the only factor considered for evaluation. The power criterion focuses merely on the theoretical calculation and ignores the actual influence after jamming, thus great limitations for evaluation.
3) *Efficiency criterion:* The mentioned information and power criteria have no considerations about the jamming effect on SAR image interpretation. Considering these

Manuscript received June 29, 2021; revised August 31, 2021 and October 18, 2021; accepted November 9, 2021. Date of publication November 22, 2021; date of current version December 10, 2021. This work was supported by the National Key Research and Development Program of China under Grant 2017YFB0502700. *(Corresponding author: Huifang Zheng.)*

Zhouyang Tang, Yunkai Deng, and Tingzhu Fang are with the Department of Space Microwave Remote Sensing System, Aerospace Information Research Institute, Chinese Academy of Sciences, Beijing 100094, China, and also with the School of Electronic, Electrical and Communication Engineering, University of Chinese Academy of Sciences, Beijing 100039, China (e-mail: tangzhouyang17@mails.ucas.edu.cn; ykdeng@mail.ie.ac.cn; fangtingzhu17@mails.ucas.ac.cn).

Chunrui Yu is with the Beijing Institute of Tracking and Telecommunication Technology, Beijing 100094, China (e-mail: ycrzxc@163.com).

Huifang Zheng is with the Department of Space Microwave Remote Sensing System, Aerospace Information Research Institute, Chinese Academy of Sciences, Beijing 100094, China (e-mail: bluebird_855@126.com).

Digital Object Identifier 10.1109/JSTARS.2021.3129494

facts, the efficiency criterion is mainly based on comparing the change of the tracking ability or target detection before and after being jammed. In [22], the jamming effect is evaluated according to the degree of deviation between the jammed centroid trajectory and the normal one without jamming. However, this method is suitable for moving targets only and needs a series of SAR images for comparison. Shi *et al.* [23] and Shen *et al.*[24] employ detection performance under jamming condition for effect evaluation. They only consider detecting real targets under suppressive jamming at the simplistic experiment condition, and the deception of deceptive jamming is ignored.

In general, the above three aspects are based on the suppression effects of jamming on SAR images. Note that the high-fidelity false targets generated by deceptive jamming can not only affect the feature extraction of SAR images, but also confuse the SAR interpretation. Besides, the existence of false targets at some local areas of the SAR image can only cause relatively minor change to the overall image quality, even under nonideal factors. Therefore, the influence of deceptive jamming cannot be effectively and reasonably measured by the aforementioned traditional methods. Besides, in [25], multifeature fusion is introduced to classify false targets into the corresponding error levels for evaluation. However, the influence of false targets' fusing into the SAR image of the adversary is not considered, so the evaluation result is not intuitive.

Consequently, more consideration should be given to the influence of false targets on SAR interpretation. Specifically, detection, recognition, and semantics are exactly what need to be considered. So far, a number of studies have made corresponding contributions to such three aspects, which are applied to traditional SAR interpretation without considering the deceptive jamming.

1) For target detection, cell-averaging constant false alarm rate (CFAR) and two-parameter CFAR (TP-CFAR) are commonly used due to their simplicity of implementation [26]. Besides, characterizing the clutter by two parameters (mean and standard deviation), TP-CFAR is proved to be useful in the nonhomogeneous state but with inevitable false alarms [27]. Considering such situation, morphological processing and median filtering are used to eliminate the false alarms in [28]. Pixel-by-pixel operations mean a high computational complexity. For higher efficiency, two-stage CFAR is considered in [29], but it cannot guarantee a satisfactory false alarm rate.
2) For deep-learning-based recognition, the dataset universally plays the core role in training and classification. In conventional tasks of SAR target recognition, existing datasets are used directly [30]–[32]. However, in our deceptive jamming evaluation issue, preprocessing of the existing SAR dataset, including jamming signal generation and 2-D windowing, is required to meet specific requirements.
3) As a high-level vision, semantics is widely considered in SAR image semantic segmentation, but their specific implementations are often complex [33], [34]. For convenience, semantic analysis can be accomplished by simply distinguishing the statistical characters of different scenarios. As a metric for comparing two statistical distributions, the Kullback–Leibler divergence (KLd) is researched and can be understood as the relative entropy [35]. Revealing that the KLd is asymmetric and unbounded, Lin [36] proposed the Jensen–Shannon divergence (JSd). The JSd can be thought as a symmetric and bounded version of the KLd and is, thus, more commonly used.

Considering the aforementioned issues, a novel visual consistency (VC)-based framework is proposed for evaluating the deceptive jamming effect on SAR along with the corresponding metrics system. As for VC, the core consideration is the consistency of responsive behaviors between generated false targets and real targets in SAR image interpretation. Fully considering the high fidelity of deceptive jamming, three levels of vision are considered in our VC-based evaluation, namely detection, recognition, and semantics. Detection and recognition are used to analyze the degree of consistency in geometric and textural features, and responsive results during the corresponding processing flows are employed for evaluation. Additionally, a novel concept, named semantic accuracy, is proposed to describe and evaluate the location rationality of false targets.

The novelty of our evaluation framework is multifaceted. Overall, a novel framework that can effectively evaluate the effect of deceptive jamming is proposed with special processing flows. Looking specifically at each visual level, there are also corresponding novelties integrated into the implementation. A novel two-stage-two-parameter CFAR (TSTP-CFAR) is proposed for the detection flow of our evaluation framework, where the normalized moment of inertia (NMI) will be used for further suppression of false alarms. Therefore, higher efficiency and lower false alarm rate can be simultaneously satisfied. Meanwhile, for the special mission of deceptive jamming evaluation, a novel and specific scheme for generating the deceptive jamming dataset is presented in the proposed recognition flow. In addition, to prevent network overfitting on the jamming template, a convolutional neural network (CNN) with batch normalization (BN) layers [37] is designed for the recognition process for multiclass problems. Besides, 2-D windowing should be applied to each input of our CNN, which further reflects the uniqueness of our proposed recognition flow. Additionally, considering the simplicity and convenience [38], [39], template matching is also employed for the two-class classification case. Finally, JSd-based semantics evaluation is introduced into our evaluation framework for the first time, which is implemented by comparing the statistical properties of the current background with that of the corresponding background templates.

In summary, the main contributions of this article are threefold.

1) A novel VC-based evaluation framework is proposed, which consists of three levels of vision, i.e., detection, recognition, and semantics. Subtle changes of deception presented by false targets can be keenly depicted.

2) Well-designed detection and recognition flows are especially provided to ensure the validity of the VC-based evaluation. Moreover, the unprecedent concept of semantic accuracy is introduced by analyzing the position rationality of false targets via JSd.
3) Responses of the evaluation framework for different deceptive jamming under varying nonideal conditions are analyzed to further verify its practicability and superiority.

The rest of this article is organized as follows. Section II mainly describes the mechanisms of deceptive jamming, along with the influence analysis caused by parameter measurement errors. Section III presents the proposed evaluation framework and the implementation details, including metrics definitions and the specific operation process. Experimental results and analysis are contained in Section IV. Finally, Section V concludes this article.

II. Signal Generation and Error Analysis of Deceptive Jamming

A. Principles of Deceptive Jamming

The generation of deceptive jamming requires strict calculation of the time delay and phase modulation, so as to generate the desired false target in the preset position. Repeater jamming is accomplished by modulating the intercepted SAR signal according to preset false target information and then retransmitting back to SAR [6], [10]. Benefiting from the intercepted signal, relatively little prior information of SAR is required for the repeater jammer, and the key reconnaissance parameters are fewer. Note that the closest slant range and velocity are important parameters for jamming modulation. Besides, if more prior information is available, or the obtained reconnaissance parameters are more comprehensive and accurate, the false image jamming can be used to jam SAR more flexibly. The complete and realistic jamming signal can be generated in advance and then transmitted to SAR in a single-trip manner once the target area is illuminated by the main lobe [40]. Note that there is no intercepted signal needed and the false image jammer can be located at either the main lobe or the sidelobe of SAR.

For a repeater jammer, the intercepted signal is often assumed only available when the jammer is irradiated by the SAR main lobe, which results in the difference in the Doppler time–frequency domain between the jamming signal and the real SAR echo [6]. While the false image jamming, which owns more complete reconnaissance parameters, is not limited on whether the jammer is irradiated by the main lobe or not, thus more flexible. However, the more stringent requirements for reconnaissance, in turn, make it more difficult to implement in practice. At present, most of the existing deceptive jamming generation methods are based on the above two typical ways.

B. Influence of Parameter Measurement Error on Deceptive Jamming

The fidelity of deceptive jamming is directly related to its coherence with the SAR signal in azimuth and range dimensions simultaneously. When countering a linear-frequency-modulated (LFM) SAR, which obtains high resolution by matched filtering, the degree of jamming signal's matching with the frequency modulation (FM) rate is an important factor. This affects the coherence as well as the focusing performance. Consider the transmitted LFM signal

$$S(\tau) = \omega_r(\tau) \exp\left(j2\pi f_0 \tau + j\pi K_r \tau^2\right) \tag{1}$$

where $\omega_r(\tau)$ denotes a window function, τ represents the fast time along the range dimension, f_0 is the carrier frequency, and K_r is the FM rate. Assume that there is an offset of FM rate ΔK; then, the corresponding spectrum at the baseband is formulated as

$$\begin{aligned} S(f) &= \text{rect}\left(\frac{f}{|K+\Delta K|T}\right) \exp\left(-j\pi \frac{f^2}{K+\Delta K}\right) \\ &\approx \text{rect}\left(\frac{f}{|K|T}\right) \exp\left(-j\pi \frac{f^2}{K}\right) \exp\left(j\pi \frac{\Delta K f^2}{K^2}\right) \end{aligned} \tag{2}$$

where rect$(\cdot)$ denotes the rectangular window function. For the sake of brevity, the constant term caused by the time delay is ignored, which does not affect the problem explanation. Afterward, the spectrum of matched filtering function corresponding to the LFM signal shown in (1) is chosen as

$$H(f) = \text{rect}\left(\frac{f}{|K|T}\right) \exp\left(j\pi \frac{f^2}{K}\right). \tag{3}$$

Note that the matched filtering function is designed according to the ideal received LFM signal; thus, the correct value of K is used. Therefore, the output of matched filtering in the frequency domain is obtained as

$$\begin{aligned} S_{mf}(f) &= S(f)H(f) \\ &= \text{rect}\left(\frac{f}{|K|T}\right) \exp\left(j\pi \frac{\Delta K f^2}{K^2}\right). \end{aligned} \tag{4}$$

Finally, the output of matched filtering in the time domain can be modeled as

$$S_{mf}(\tau) = K \int_{-T/2}^{T/2} \exp(j\pi \Delta K z^2) \exp(-j2\pi K \tau z)\, dz. \tag{5}$$

As similarly mentioned in [41], there will be a phase error of $\pi \Delta K T^2/12$ at the compressed peak, resulting in corresponding defocus. Back to false targets generation, once the jitter of FM rate occurs when processing the jamming signal, the corresponding phase error and defocus will appear, which affect the verisimilitude and confusion of false targets.

In consideration of azimuth coherence, the accurate measurement of platform kinematic parameters plays a key role. Taking repeater jamming as an example, the effects of measurement error in the closest slant range and velocity are analyzed here. According to [6] and [10], slant range difference $\Delta R(\eta)$ corresponding to a false target at R_t with η_t with the second-order Taylor expansion is

$$\begin{aligned} \Delta R(\eta) &= 2(R(\eta - \eta_t) - R_J(\eta)) \\ &\approx 2(R_t - R_J) + \frac{x_t^2}{R_t} - \frac{2x_t v \eta}{R_t} + \left(\frac{1}{R_t} - \frac{1}{R_J}\right) v^2 \eta^2 \end{aligned} \tag{6}$$

where $R(\eta-\eta_t)$ and $R_J(\eta)$ are, respectively, the instantaneous slant range of the preset ideal point target and the jammer. R_t and R_J present the closest slant range between SAR and, respectively, the preset false target and jammer. η is the slow time along the azimuth dimension, v is the velocity, and $x_t = v\eta_t$. Clearly, the closest slant range contributes to both the first-order term and the second-order term, and so does velocity. The former has an effect on positioning in azimuth, whereas the latter determines the focusing performance of generated false targets. Specifically, the second-order term is used for compensation to obtain the Doppler FM rate required at the target point with R_t. Here, the compensating Doppler FM rate is defined as

$$K_{\text{com}}(R_0, v) = \frac{2v^2}{\lambda}\left(\frac{1}{R_t} - \frac{1}{R_J}\right). \tag{7}$$

Whenever a closest slant range or velocity measurement error occurs, there will be a Doppler FM rate error $\Delta K_{\text{com}}(R_0, v)$ caused by ΔR_0 or Δv. Review the phase error mentioned in (5); the inevitable Doppler phase error will cause degradation to image quality along azimuth.

From the above analysis, we can see that the focusing performance of false targets is largely dependent on the mentioned parameters. Different levels of measurement errors result in correspondingly weakened confusion of deceptive jamming in SAR images. However, such a phenomenon cannot be reasonably evaluated by traditional metrics. For effective evaluation, a reliable and logical evaluation method is urgently needed. With the reasonable evaluation results, survivability in complicated electromagnetic environments can be analyzed from the perspective of SAR, and feedback can be provided for jamming configuration optimization from the perspective of jammer.

III. Proposed Evaluation Framework and Its Implementation Details

In SAR electronic countermeasures (ECMs), the most important feature of the deceptive jamming lies in its ability to generate false targets. Superior to the suppressive jamming, which can only obscure SAR images by transmitting high-power jamming signals, deceptive jamming is aimed at generating false targets to simulate the real ones for confusion. In order to effectively evaluate the deceptive jamming effect on SAR, objective and effective evaluation methods play a decisive role. However, these are difficult, and few references are left. Traditional evaluation metrics all consider the change of image quality, which are suitable for suppressive jamming but not the deceptive jamming especially with high fidelity. With the gradual improvement of reconnaissance accuracy, the fidelity of deceptive jamming to SAR is correspondingly improved, showing better deceptive properties in SAR images. Nevertheless, traditional evaluation metrics have no considerations on the verisimilitude of false targets, making their evaluation results unreliable. Therefore, the research should focus more on improving the ability to evaluate the deception caused by false targets.

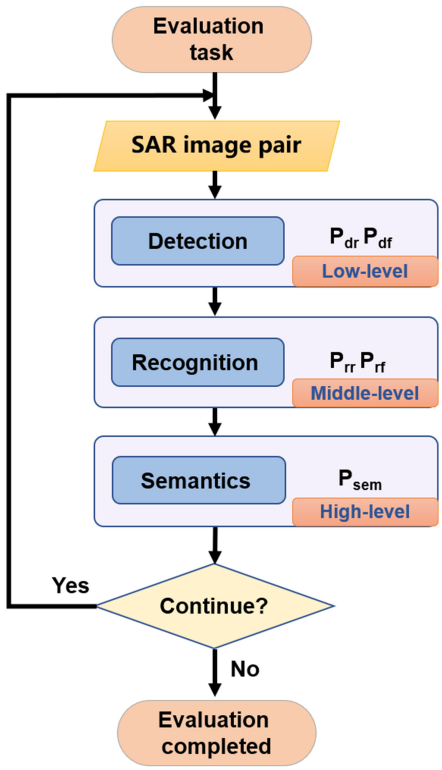

Fig. 1. Proposed VC-based evaluation framework and corresponding metrics in different levels of vision.

A. Framework Panorama

On the SAR battlefield, the commander needs to make tactical adjustment according to the real-time situation, such as the distribution and number of military targets in the combat zone, of which the foothold lies in target detection and recognition. As an efficient means of ECM, deceptive jamming has the potential to confuse the situational awareness via high-fidelity false targets. By evaluating the corresponding influence on the adversary, the effectiveness of deceptive jamming can be analyzed.

Considering the above issues, a novel VC-based evaluation framework for deceptive jamming is proposed from the perspective of SAR image interpretation. The entire scheme is shown in the block diagram in Fig. 1, which clearly illustrates three levels of vision considerations and the corresponding metrics. The SAR image pair to be processed is successively input for target detection and recognition, and the successfully recognized false targets further go through the semantic validation for analysis of the background rationality. Finally, the evaluation ends with calculating quantitative metrics, which are used to describe the influence of deceptive jamming on SAR images. The specific definitions of the adopted metrics and their practical implications are explained as follows.

1) Detection Probability: Detection probability of real targets (P_{dr}) and false targets (P_{df}) is defined as

$$P_{\text{dr}} = \frac{N_{\text{det}} - N_{\text{df}}}{N_{\text{real}}} = \frac{N_{\text{dr}}}{N_{\text{real}}}$$

$$P_{\mathrm{df}} = \frac{N_{\mathrm{det}} - N_{\mathrm{dr}}}{N_{\mathrm{false}}} \tag{8}$$

where N_{real} and N_{false} denote the number of preset total real and false targets, respectively. N_{det} presents the total number of successfully detected targets, including both the real ones and the false ones. N_{dr} and N_{df} are the number of successfully detected real targets and false ones, respectively. In experiments, P_{dr} can be acquired by comparing the detection results of real targets in images before and after interference. More specifically, the jamming-free image, where the included targets are considered as the real targets, is first input into the detection flow; then, the number and position of the detected real targets are recorded and used as a reference. Afterward, the targets detected in the jammed SAR image are, then, compared with the just mentioned reference, and the targets that appear in both detection results are thought to be the successfully detected real ones. Thereby, the corresponding number N_{dr} is obtained. Ultimately, the metrics P_{dr} and P_{df} are both available. The former is used to analyze the deceptive jamming effect on the detection of real targets, whereas the latter is adopted to evaluate the fidelity of false targets at the low-level vision. The larger the metric P_{df} is, the higher fidelity the false targets have, indicating the more successful deception on SAR images.

2) Recognition Probability: Based on above detection results, recognition is further conducted for the incoming SAR image pair. Recognition probability of real targets (P_{rr}) and false targets (P_{rf}) is defined as

$$\begin{aligned} P_{\mathrm{rr}} &= \frac{N_{\mathrm{rec}} - N_{\mathrm{rf}}}{N_{\mathrm{real}}} = \frac{N_{\mathrm{rr}}}{N_{\mathrm{real}}} \\ P_{\mathrm{rf}} &= \frac{N_{\mathrm{rec}} - N_{\mathrm{rr}}}{N_{\mathrm{false}}} \end{aligned} \tag{9}$$

where N_{rec} denotes the total number of successfully recognized targets, and N_{rr} and N_{rf} are the number of successfully recognized real targets and false ones, respectively. The definitions of N_{real} and N_{false} are the same as mentioned earlier. Compared to the preset categories of real targets, N_{rr} can be obtained in the similar manner to N_{dr}; then, both P_{rr} and P_{rf} are obtained. Similarly, P_{rr} considers the masking effect of deceptive jamming on real targets, while P_{rf} is used to evaluate the verisimilitude of generated false targets at the middle-level vision, which considers their confusion over SAR interpretation. If the false targets have similar responsive behaviors toward the detection and recognition flow as the real ones, they will be more likely to be detected and recognized. In other words, a larger P_{rf} indicates that the false targets are of higher fidelity.

3) Semantic Accuracy: As for high-fidelity false targets, they are more likely to adapt to the detection and recognition, resulting in confusion. However, for those false targets generated in wrong background, which means their contradicting common sense, the corresponding deceptive jamming still should be considered unsuccessful. For example, ships are unlikely to be on land. At this time, even deceptive jamming passed the test of detection and recognition with high fidelity, it should still be considered inappropriate.

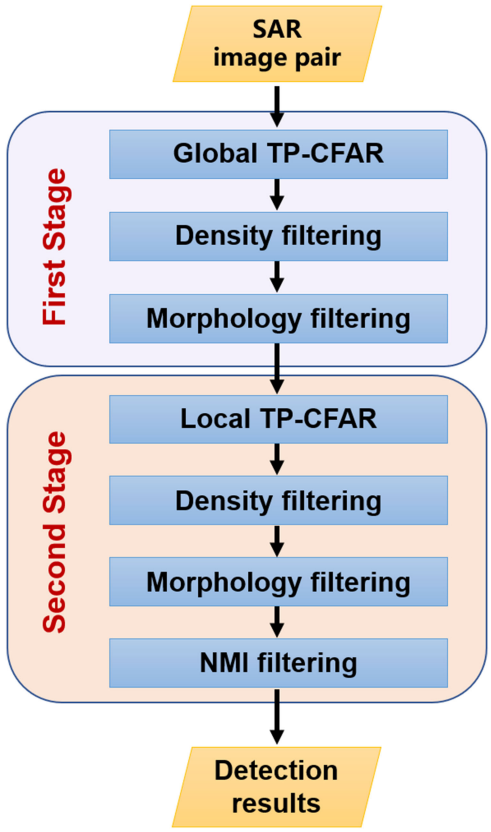

Fig. 2. TSTP-CFAR-based detection flow.

In order to quantitatively evaluate the rationality of deceptive jamming at the semantic level, a novel concept, semantic accuracy, is proposed here for considering whether false targets can fit into the context. Semantic accuracy is defined as

$$P_{\mathrm{sem}} = \frac{N_{\mathrm{rf}} - N_{\mathrm{sem}}}{N_{\mathrm{false}}} \tag{10}$$

where N_{sem} is the number of semantically incorrect false targets. Therefore, $N_{\mathrm{rf}} - N_{\mathrm{sem}}$ means the number of false targets with correct semantics, which is obtained from the successfully recognized ones. The acquisition of N_{sem} will be described in subsequent sections in detail.

B. Detection Considerations

To ensure that the evaluation framework works correctly and practicably, an effective target detection flow is rather important, which is directly related to the acquisition of P_{dr} and P_{df}. Therefore, TSTP-CFAR is proposed for satisfactory detection performance, whose processing flow is shown in Fig. 2.

First, an original jamming-free SAR image is input and then processed by the global TP-CFAR. The whole image is treated as a large sliding window, and the contained pixels are detected using a uniform threshold. Implementation details of TP-CFAR can refer to [27]. After global TP-CFAR, a lot of detected points can be obtained as candidates, including both the real target points and the false alarm points. Without further operation, the detection result will contain a lot of false alarms. Note that

the points belonging to the target are closer to each other and clustered within a limited range, which can present the general outline of the target. However, false alarms are distributed more randomly and dispersively. Therefore, density filtering is subsequently considered. Specifically, with the current point being the filtering center, if the number of detected points in the filtering window is less than 1/4 of the points contained in the filtering window, the points around this center point are considered to be scattered. Then, the current center point will be removed as a false alarm point. After considering all the candidate points, several relatively concentrated groups of points will be left, which roughly reflect the target shapes. Afterward, each point group will be transformed into the corresponding connected region through morphological filtering, namely erosion and dilation [42], [43], to represent a possible target. These operations form the first stage of detection, of which the processed result acts as the input of the local TP-CFAR in the second stage.

Note that the global TP-CFAR in the first stage is used to quickly obtain the preliminary locations of candidate targets, but this may leave several false alarms of connected regions and lose the outline details of some targets. Therefore, the local TP-CFAR is considered successively. The detected pixels of stage one are taken as the centers to obtain outwardly extended areas for successive detection. The extended areas can be chosen as large as the size of the targets to be processed. Pixels contained in the extended areas, which are much fewer than the total pixels in the original image, are taken as the detection objects of TP-CFAR. Compared with a direct usage of TP-CFAR, the target contour can be better presented, and the calculation can be greatly reduced. Following the local TP-CFAR, density filtering and morphology filtering are likewise carried out. Besides, if false alarms are not handled completely, they will also appear as connected regions and then affect the final detection results. Notably, the NMI values of connected regions corresponding to targets with similar size are close to each other, while the false alarms are with irregular size, which can be further removed in view of NMI outliers. NMI can be defined as [44]

$$\mathrm{NMI} = \sum_{m=1}^{M} \sum_{n=1}^{N} A(m,n) \cdot r^2 \tag{11}$$

where M and N denote the slice size and $A(m,n)$ denotes the value of a certain pixel in the target slice, with r being its distance to the target centroid (m_c, n_c), which is formulated as

$$r = \sqrt{(m-m_c)^2 + (n-n_c)^2}. \tag{12}$$

Up to this point, the aforementioned detection procedure reduces false alarms to a significantly low level, which guarantees the validity and accuracy of the evaluation framework. Afterward, the jammed SAR image is input into the TSTP-CFAR detection flow and goes through the similar two-stage processing as the origin SAR image does. Finally, the metrics P_{dr} and P_{df} can be obtained, and effect evaluation for deceptive jamming in the low-level vision via detection is achieved.

C. Recognition Considerations

1) Template-Matching-Based Target Recognition: The template used for matching can be generally divided into image template and feature template. The former is based on the SAR image template directly, which compares the test image to be classified with the image template to find the closest category. However, a direct difference measurement using image pixels is not robust enough for situations such as rotation and displacement [45]. Better performance can be obtained by extracting descriptive feature of the images as feature templates for recognition, which is a brief but effective method. As described in [44], NMI has the feature of rotation, scaling, and translation invariability; hence, the NMI feature of a certain region of interest ($\mathrm{NMI_{ROI}}$) is extracted and compared with the NMI of the template ($\mathrm{NMI_{tem}}$).

The template that matches the category of targets within the current regions of interest (ROIs) should be selected first. The detected connected regions in the jamming-free SAR image will be compared with multiple types of target templates based on the feature distance. The feature can be chosen as a quantity that can describe the characters of a region, such as NMI. Thereupon, the targets in detected connected regions are categorized based on the following rule:

$$C = \min\left(D_1, D_2, D_q, \ldots, D_Q\right) \tag{13}$$

with

$$D_q = \mathrm{mean}\left(\left|\frac{\mathrm{NMI_{ROIs}}}{\mathrm{NMI_{temq}}} - 1\right|\right) \tag{14}$$

where $\mathrm{NMI_{ROIs}}$ and $\mathrm{NMI_{temq}}$ denote the NMI feature of the chosen ROIs and the target template of the qth category, respectively. The difference between the two can be measured according to (14), thus obtaining D_q. Afterward, the category of targets within ROIs, denoted as C, can be determined by the minimum feature distance via comparing to different types of templates. Once the matched target template is determined, the corresponding template will, in turn, be used for recognition of the targets within detected ROIs in the jammed SAR image based on a decision threshold. Considering that what counts is the deviation degree relative to NMI of the template, the recognition distance is defined as follows:

$$D_{\mathrm{rec}} = \left|\frac{\mathrm{NMI_{ROI}}}{\mathrm{NMI_{tem}}}\right|. \tag{15}$$

The smaller the recognition distance D_{rec} is, the closer the NMI features of the two are, and the more the corresponding ROI region matches the target template. Therefore, once the recognition distance is below the preset threshold value, the target in the ROI is considered to be the same category as the template to be compared.

Back to the evaluation process, according to the obtained detection results, the position information about the detected targets is recorded, based on which the corresponding ROIs are successively segmented and obtained. The target category is determined based on the recognition distance between ROIs and the chosen template. For the ROIs that are judged to contain real targets, their recognition results will be compared

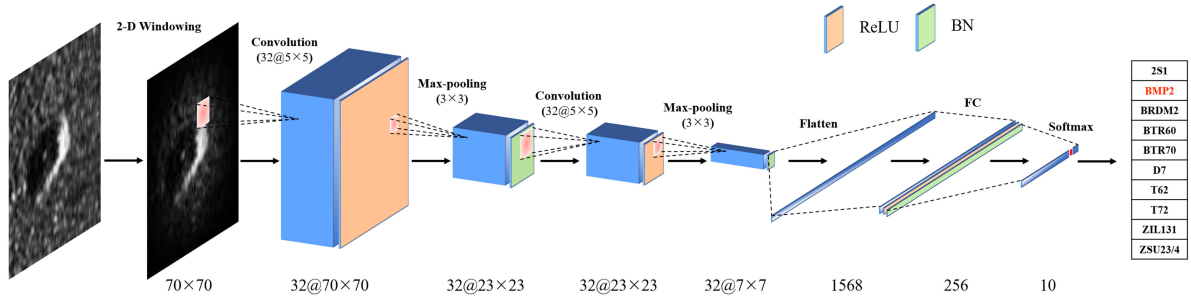

Fig. 3. Specifically designed CNN structure for fine classification.

with the ground truth of preset targets; then, N_{rr} can be obtained. Furthermore, P_{rr} and P_{rf} are successively available based on (9).

2) CNN-Based Target Recognition: In order to guarantee the successful implementation of recognition related evaluation, an effective CNN structure is specifically designed for a multiclass recognition task, as shown in Fig. 3. For feature extraction, an input 70×70 image first goes through a convolution layer with 32 5×5 convolution kernels, forming the corresponding feature maps. Then, an activation layer with the rectified linear unit (ReLU) is employed to inject nonlinearity into the network for better performance and faster convergence. Followed by a max-pooling layer with pooling size 3×3, the scaled feature maps are obtained, which not only serves to reduce the number of network parameters, but also expands the receptive field of subsequent connections. Afterward, a BN layer is used for accelerating the training speed by adjusting the distribution of input data of different layers to a relatively stable level, which is also an effective regularization method of preventing overfitting [37]. After this, a pair of convolution and max-pooling are considered in the same manner as mentioned. Considering that the same receptive field can be obtained with fewer parameters by stacking several small convolution kernels, the convolution kernels with 5×5 are chosen. Besides, the increased network nonlinearity obtained by stacking operation can provide better performance improvement [46], [47]. Afterward, a flatten layer is used to spread out the feature maps, where the dropout operation with probability 0.5 is considered for reducing overfitting [37]. Successively, a fully connected layer attached with a ReLU activation layer and a BN layer is used for feature integration, and the dropout operation with probability 0.65 is considered. Finally, a softmax activation layer is employed for recognition with the cross-entropy loss function. Note that during the training stage, the input images are from the 2-D windowed jamming dataset, which will be introduced in the following part in detail. Each input image is a grayscale image with a size of 70×70, which will first be normalized. In the evaluating stage, the detected ROIs act as the input of the CNN. Before recognition, each ROI should go through the 2-D windowing and normalization operations for preprocessing, which helps reduce overfitting and improve identification performance. For both training and evaluating stages, the output of the network is the classification result of the input, and the specific category is given, namely a certain type of tanks.

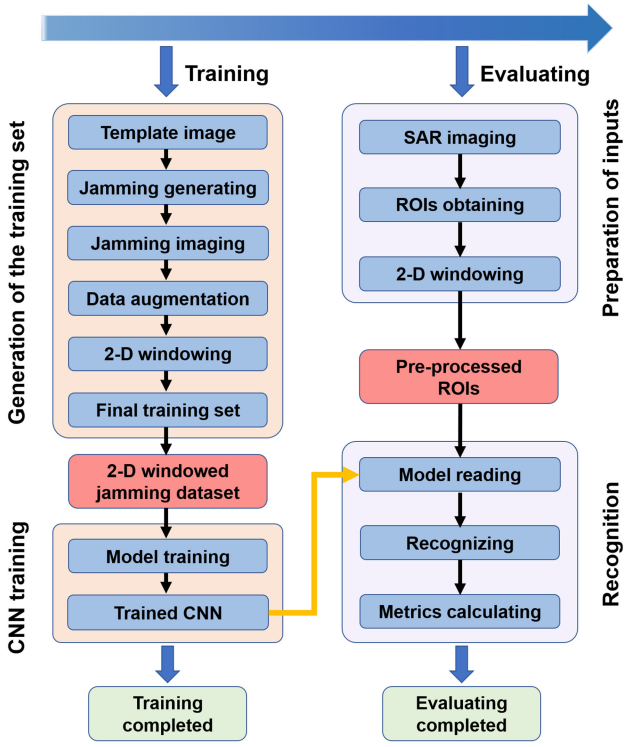

Fig. 4. CNN-based recognition flow.

The detail recognition flow is illustrated in Fig. 4, which is clearly divided into two parts: training and evaluating. The training part consists of generation of the training set and CNN training. Several innovative considerations are included in the dataset generation. The existing dataset is directly used in conventional tasks of SAR target recognition. However, for deceptive jamming evaluation, the original SAR dataset is used to generate the deceptive jamming signal based on the geometric model first. Afterward, a certain SAR imaging algorithm is chosen to form the deceptive jamming in the image domain, and the basic training dataset of false targets is, thus, built. This is one of the novel points about the generation of the jamming dataset. Besides, it is widely known that the amount of dataset is an important factor to ensure the performance of the CNN. Unfortunately, the basic templates in the existing SAR dataset used for training are not sufficient. In order to increase the diversity of the dataset and improve the performance of recognition, rotation and

translation can be considered on the original training dataset and, thus, the corresponding data augmentation. As another aspect of innovation, 2-D windowing will be performed to the extended dataset. This is because when deceptive jamming templates are directly incorporated into the SAR scene, they will usually appear abrupt due to the inconsistency between the edges of the template image and the background. Through 2-D windowing, the edges of the template image will become smoother and blend better with the background in SAR images. Besides, possible overfitting caused by the background in the template image on the recognition can concurrently get an effective reduction. Afterward, the 2-D windowed jamming dataset is input into the employed CNN for network training. Notably, the reduction of overfitting is also considered in terms of the CNN structure. For the consideration of avoiding overfitting in the problem of deceptive jamming effect evaluation, BN layers are introduced into our designed CNN [37]. Furthermore, note that the jamming dataset is of small scale, and the input ROI obtained after the detection flow is of small size with 70×70. Under the premise of performance assurance, two pairs of convolution layer with 32 5×5 convolution kernels and pooling layer are used to avoid overfitting.

Consecutively, the evaluating part is conducted based on the detected ROIs, which contain targets for recognition. Acting as the input of our CNN for the specific jamming evaluation task, the detected ROIs should first go through the 2-D windowing operation for two reasons. The first one lies in that 2-D windowing can better reduce the influence of the background around ROIs on recognition, and the second one is to match the 2-D windowed training dataset. The above considerations reflect the uniqueness of our recognition task. When the target slices for recognition are ready, the trained CNN from the training part is, thus, read in for recognizing. Finally, the evaluation is ended with recognition-related metrics calculation, namely P_{rr} and P_{rf}. The procedure of metrics calculation is similar to that based on template matching.

D. Semantic Considerations

Semantic accuracy lies on the highest level of the evaluation framework, which is used to analyze the location rationality of successfully detected and recognized false targets. The concept of semantic accuracy is defined according to the type of false target and the corresponding background. For example, ships are paired with their usual background of waters. For a certain false target, its common background template is used as the reference. The background around the false target in a SAR image is segmented out; then, the difference in statistical properties with respect to the reference will be examined. Quantitatively revealing the semantic accuracy, the high-level vision of deceptive jamming is further evaluated.

The JSd is a measure of the difference between two probability distributions [35], [36]. Here, the JSd is introduced in this article to compare the statistical characteristics of the background around the false target with the corresponding reference, thus obtaining the semantic accuracy. Mathematically, the JSd is defined as

$$\text{JSd}\left(G_t\|G_m\right)=\frac{1}{2}\text{KLd}\left(G_t\|\frac{G_t+G_m}{2}\right)+\frac{1}{2}\text{KLd}\left(G_m\|\frac{G_t+G_m}{2}\right) \tag{16}$$

with

$$\text{KLd}\left(G_x\|G_y\right)=\sum_{i}^{I}G_x(i)\log_2\frac{G_x(i)}{G_y(i)} \tag{17}$$

where KLd denotes the Kullback–Leibler divergence. G_t and G_m are, respectively, the gray histogram of the background of a false target to be processed and its corresponding background template. i is the ith value of the gray histogram. The KLd commonly considers the normalized frequency distribution in calculation, while neglecting the influence of the gray value. This will be subject to performance restriction in the occasions where the amplitude information of an image is important. Therefore, we recommend to measure the similarity of different distributions with the gray-value-weighted KLd

$$\text{KLd}\left(G_x\|G_y\right)=\sum_{i}^{I}i\cdot G_x(i)\log_2\frac{G_x(i)}{G_y(i)}. \tag{18}$$

The smaller the value of the JSd, the higher the similarity of the two compared statistical distributions. Once the obtained JSd is smaller than the preset threshold, the background of the false target to be measured is thought to be similar to its corresponding common background template. At this time, the false target is considered to be in a reasonable background and, thus, the correct semantics. Deceptive jamming with small JSd indicates the outstanding VC relative to the real target in view of simultaneously geometric features, textural features, and high-level semantic rationality. A false target with such features can cause extremely high deceptive confusion. As for metrics calculation, by judging the semantic rationality of all the successfully recognized false targets, N_{sem} can be obtained via counting up all the semantically incorrect false targets. Then, P_{sem} is available according to (10). At this point, the entire evaluation framework has been fully implemented, and the metrics are all obtained.

IV. Experiment and Analysis

In this section, a series of experiments are conducted to verify the effectiveness and practicability of the proposed evaluation framework. First, a comparative experiment on detection is considered to demonstrate the superiority of our TSTP-CFAR. Afterward, the validity of the CNN for recognition related evaluation is demonstrated, along with the corresponding templates generation. Besides, the ability of the JSd to distinguish different gray statistical characteristics is verified and analyzed. Furthermore, two types of deceptive jamming, namely repeater jamming and false image jamming, are generated to verify the outstanding and reasonable evaluation framework. What is noteworthy is that for both types of deceptive jamming, several possible nonideal situations in reality are analyzed and experimented in

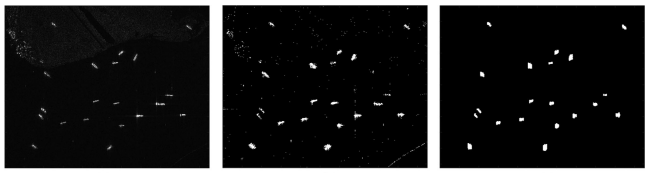

(a) (b) (c)

Fig. 5. Comparison of detection performance. (a) SAR image to be detected. Detection results obtained by (b) TP-CFAR and (c) the proposed TSTP-CFAR.

detail, including closest slant range measurement error, velocity measurement error, varying signal-to-noise ratios (SNRs), and varying resolutions.

A. Preparatory Work

1) Detection Performance Verification of TSTP-CFAR: In order to conduct the experimental analysis of the advantages of our proposed TSTP-CFAR in detail, the detection performance of TP-CFAR and TSTP-CFAR is compared via the experiment. As shown in Fig. 5(b), although TP-CFAR can detect targets in SAR images, it contains a large number of false alarms. The false alarms are caused by strong scattering points of some nontarget objects on one hand. On the other hand, they are also related to the speckle in the SAR image. Meanwhile, the aggregation of target contour detected by TP-CFAR is not satisfactory, which is not conducive to subsequent operations. In addition, TP-CFAR considers all the pixels of the image through the sliding window, which needs a large amount of calculation. To solve these problems, TSTP-CFAR is proposed with two stages of operations, where density filtering and morphology filtering are considered for false alarm suppression. Moreover, the connected regions of false alarms will further be identified and removed in view of NMI outliers. The corresponding detection result is shown in Fig. 5(c), and the outstanding performance of TSTP-CFAR is illustrated by the excellent result of target detection and false alarm suppression. Besides, for the SAR image with a size of 1024×1050, the operation time needed for TSTP-CFAR is 50.7 s, which is much smaller than that of TP-CFAR with 163.1 s.

2) Recognition Performance Verification of the CNN: Based on the flowchart shown in Fig. 4, recognition performance of the adopted CNN is verified here. The public Moving and Stationary Target Acquisition and Recognition (MSTAR) dataset is used here for performance discussion and method validation, which is provided by the MSTAR project funded by both Defense Advanced Research Projects Agency and Air Force Research Laboratory [30]. The dataset contains SAR images of different military targets obtained by an X-band airborne SAR system with a resolution of 0.3 m in the spotlight mode. The template images were obtained under different pitch angles and observation angles. Images at a pitch angle of 17° are used as the training set, which contains ten types of targets, namely 2S1, BMP2, BRDM2, BTR60, BTR70, D7, T62, T72, ZIL131, and ZSU23/4, whereas images at a pitch angle of 15° are used as the testing set.

To match our task of deceptive jamming effect evaluation, several preprocessing should be done on the dataset to meet the experimental requirements. Different styles of dataset corresponding to the processing flow are shown in Fig. 6, where the first row shows the optical images. The corresponding origin SAR images are on the second row. Taking the origin SAR images as the jamming templates, based on the deceptive method of false image jamming, the deceptive jamming signals are generated and then imaged as shown on the third row of Fig. 6. Compared to the origin SAR images, the deceptive ones own similar geometrical and textural features but look slightly blurry, which is related to the employed SAR parameters of low resolution shown in Table I. Furthermore, translation and rotation are both considered for data augmentation, where a ninefold expansion is obtained by a combination of three shifts in the horizontal direction and the vertical direction, respectively. Meanwhile, a twofold increase is considered via angular rotation. As a result, the final dataset is expanded by 11 times shown in detail in Table II. Finally, 2-D windowing is implemented via a Kaiser window with β being 5, and the windowed results are presented on the last row of Fig. 6. The optimization algorithm Adam is considered for training the network. A batch size of 128 and an initial learning rate of 0.001 are chosen as recommended in [48], which is proved to own high computational efficiency and excellent convergence. Denote the mentioned ten categories of targets, respectively, as the number ranging from 0 to 9, the classification results on the testing set are shown in Table III, with an average recognition accuracy of 94.88%. Therefore, the target recognition performance of the trained CNN is sufficient to carry out the recognition-related evaluation task for deceptive jamming.

3) JSd-Based Statistical Character Analysis: In this part, several typical scenes are selected to illustrate the specific role of JSd in distinguishing statistical characters. Fig. 7 shows five different types of regions in SAR images: waters, port, factory, grass, and block of size 256×256. Fig. 8 shows the corresponding gray histograms. SAR images and histograms of different regions have certain visual differences, and the JSd is used to quantitatively calculate the statistical differences between every two of them. The calculation results are shown in Table IV, of which the visualized expression is illustrated in Fig. 9. It can be seen that the more similar the histogram is, the smaller the JSd value will be. Besides, the JSd of the image to itself is 0, indicating no differences. Take the area of waters for example; it is most similar to the port with the smallest JSd 1.837 and most different from the factory with the largest JSd 12.839, which is consistent with the intuitive visual experience. Note that the JSd calculation results are symmetric, as can be seen in both Table IV

TABLE I
PARAMETERS RELATED TO FALSE IMAGE JAMMING

Parameter	Value
Pulse Width	$2\mu s$
Sensor Velocity	110 m/s
Carrier Frequency	9.6 GHz
Signal Bandwidth	180 MHz
Sampling Frequency	234 MHz
Pulse Repetition Frequency	163 Hz

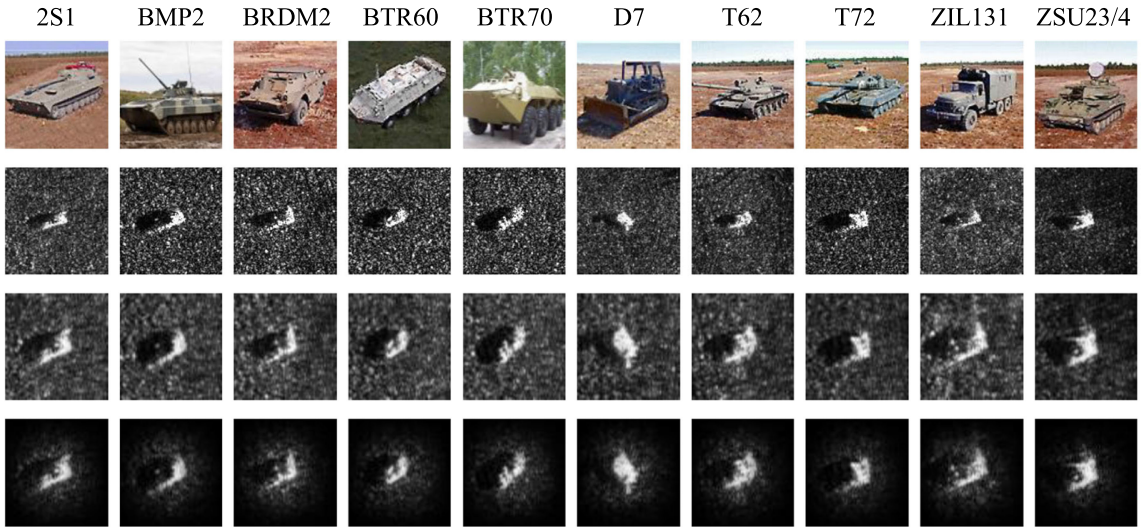

Fig. 6. Target templates and the preprocessing results. The optical images are on the first row, the corresponding SAR images are on the second row, and the imaging results of false targets before and after 2-D windowing are, respectively, on the third and last row.

TABLE II
DETAILS OF THE EXTENDED JAMMING DATASET FOR CNN CLASSIFICATION

Dataset	Target category										
	2S1	BMP2	BRDM2	BTR60	BTR70	D7	T62	T72	ZIL131	ZSU23/4	Total
Training	299×(9+2)	233×(9+2)	298×(9+2)	256×(9+2)	233×(9+2)	299×(9+2)	299×(9+2)	232×(9+2)	299×(9+2)	299×(9+2)	**2747×(9+2)**
Testing	274×(9+2)	195×(9+2)	274×(9+2)	195×(9+2)	196×(9+2)	274×(9+2)	273×(9+2)	196×(9+2)	274×(9+2)	274×(9+2)	**2425×(9+2)**

TABLE III
CLASSIFICATION RESULT OF THE ADOPTED CNN ON THE TESTING SET OF GENERATED FALSE TARGETS

	Recognition results										
	0	1	2	3	4	5	6	7	8	9	Accuracy
0	**3006**	0	0	8	0	0	0	0	0	0	99.73%
1	107	**1846**	0	101	87	0	0	4	0	0	86.06%
2	476	21	**1260**	25	17	5	0	1	0	9	81.62%
3	18	0	34	**2084**	6	0	0	3	0	0	97.16%
4	6	0	0	14	**2136**	0	0	0	0	0	99.07%
5	1	0	0	0	0	**3003**	0	0	10	0	99.64%
6	263	0	0	0	0	3	**2720**	0	17	0	90.58%
7	31	12	0	29	7	0	0	**2077**	0	0	96.34%
8	1	0	0	0	0	11	0	0	**2997**	5	99.44%
9	2	0	0	0	0	13	0	0	11	**2988**	99.14%
Average accuracy											**94.88**%

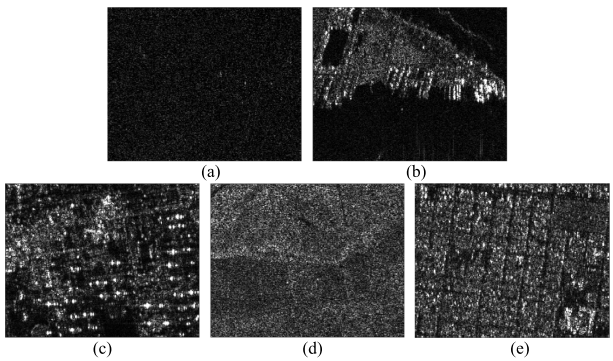

Fig. 7. SAR scenarios for statistical characteristics comparison. (a) Waters. (b) Port. (c) Factory. (d) Grass. (e) Block.

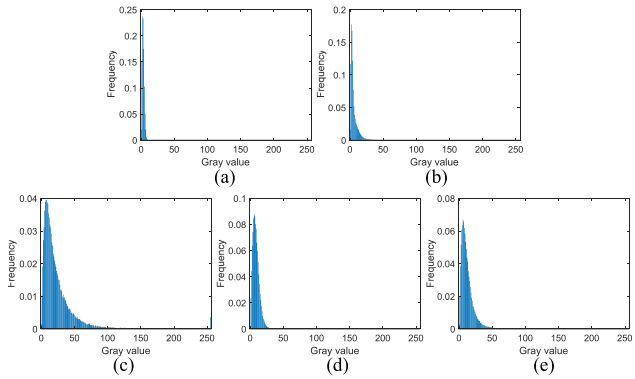

Fig. 8. Gray histograms of corresponding SAR scenarios. (a) Waters. (b) Port. (c) Factory. (d) Grass. (e) Block.

TABLE IV
COMPARISON OF STATISTICAL CHARACTERISTICS BASED ON THE JSD

Region types	JSd				
	Waters	Port	Factory	Grass	Block
Waters	0	1.837	**12.839**	3.920	6.025
Port	1.837	0	**7.697**	1.341	1.940
Factory	**12.839**	7.697	0	8.741	4.478
Grass	3.920	1.341	**8.741**	0	1.586
Block	**6.025**	1.940	4.478	1.586	0

and Fig. 9. The above experiments demonstrate the validity of JSd's distinguishing the statistical characters of different images, which lays a foundation for the semantic rationality analysis of deceptive jamming in the following section.

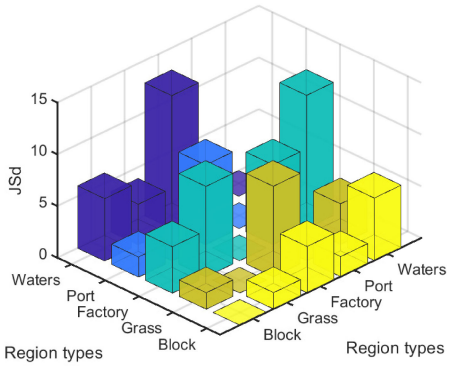

Fig. 9. Comparison results of statistical characteristics based on the JSd.

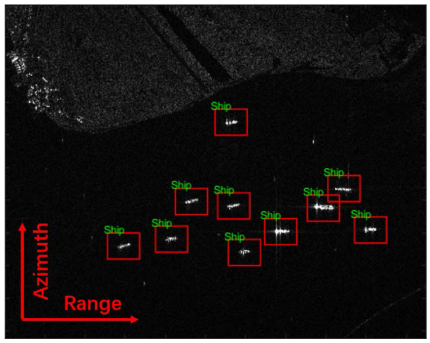

Fig. 10. Jamming-free SAR image that acts as a reference.

B. Repeater-Jamming-Based Evaluation Experiments

The deceptive-jamming-contaminated SAR images suffer from image quality degradation; more than that, the generated false targets with high fidelity will confuse the interpretation of SAR images. In order to quantitatively evaluate such effects of deceptive jamming on SAR, a number of experiments are carried out based on the repeater jamming here. Recall that repeater jamming is implemented by modulating the intercepted SAR signal, and fewer reconnaissance parameters are required. It is noteworthy that both closest slant range and velocity are two typical parameters, which play a significant role in deception performance. Therefore, measurement errors of the mentioned two parameters are considered and analyzed in detail.

The objects to be processed are the jamming-free SAR image and the corresponding jammed SAR image for evaluation. First, the detection flow is completed by TSTP-CFAR, and then, a two-class recognition task is carried out based on template matching. Then, the detection- and recognition-related metrics are obtained. For the two-class classification problem, the target is recognized as a ship or others. Furthermore, semantics rationality is considered based on the JSd to acquire the semantics accuracy as high-level vision. Finally, the whole evaluation framework is completed, giving all the adopted metrics. Meanwhile, several traditional metrics mentioned in [25], namely image entropy (H), ENL, Euclidean distance (d), correlation coefficient (ρ), and SSIM, are used for evaluation in view of SAR image quality for comparison. The detection and recognition result of the original jamming-free SAR image is shown in Fig. 10. Acting as the reference for subsequent evaluations, ten real ships are successfully detected and recognized from the scene of port. The SAR image is formed with the parameters shown in Table V from Sentinel-1, where azimuth and range lie along the vertical direction and the horizontal direction, respectively.

TABLE V
PARAMETERS RELATED TO REPEATER JAMMING

Parameter	Value
Pulse Width	$51\mu s$
Sensor Velocity	7190 m/s
Carrier Frequency	5.4 GHz
Signal Bandwidth	42 MHz
Sampling Frequency	47 MHz
Pulse Repetition Frequency	1663 Hz

1) Closest Slant Range Measurement Errors: Ten false ship targets have been added into the origin SAR image based on the deceptive mechanism of repeater jamming, and the related parameters are shown in Table V. Considering the influence of closest slant range measurement errors on deceptive jamming effect evaluation, eight levels of random errors are adopted when generating false targets, i.e., 0, 0.5%, 2.5%, 5%, 10%, 15%, 20%, and 25%. The evaluation framework is experimented, and the original jamming-free SAR image in Fig. 10 without measurement error is the reference for evaluation.

For the representation of detection and recognition results, the red boxes represent the detected real targets, and the yellow ones represent the detected false targets. The characters above the boxes denote the recognized category. In addition, correct and incorrect recognition results are denoted with green and yellow characters, respectively. Meanwhile, for false targets that can be successfully detected and recognized, semantic accuracy is further analyzed to determine the logical correctness of their location. For example, it is unlikely that a ship is on land or several ships are too close in real life. The targets that violate these logic should be considered in an unreasonable context, which will be marked in a green box.

As shown in Fig. 11, the imaging quality of the false targets gradually deteriorates with the increase in the closest slant range measurement error, which is especially evident in azimuth direction, i.e., the vertical direction. Note the fact that the closest slant range directly affects the azimuth Doppler FM rate of the received signal, as derived in (7). A larger closest slant range measurement error corresponds to a more serious Doppler FM rate mismatch with the azimuth matched filter, resulting in a gradual decline in focusing performance. This corresponding defocus directly affects the feature extraction of false targets, which is, hence, reflected in the detection and recognition results.

As illustrated in Fig. 12, the detection results of false targets do not change with the increasing measurement error of closest slant range, and so does the detection and recognition results of real targets. However, when larger errors exist, the recognition performance of false targets and their semantic accuracy are correspondingly affected, which are described by the red-dotted line and the green-dashed dotted line, respectively. This illustrates the necessity to introduce vision of higher level. Besides, the

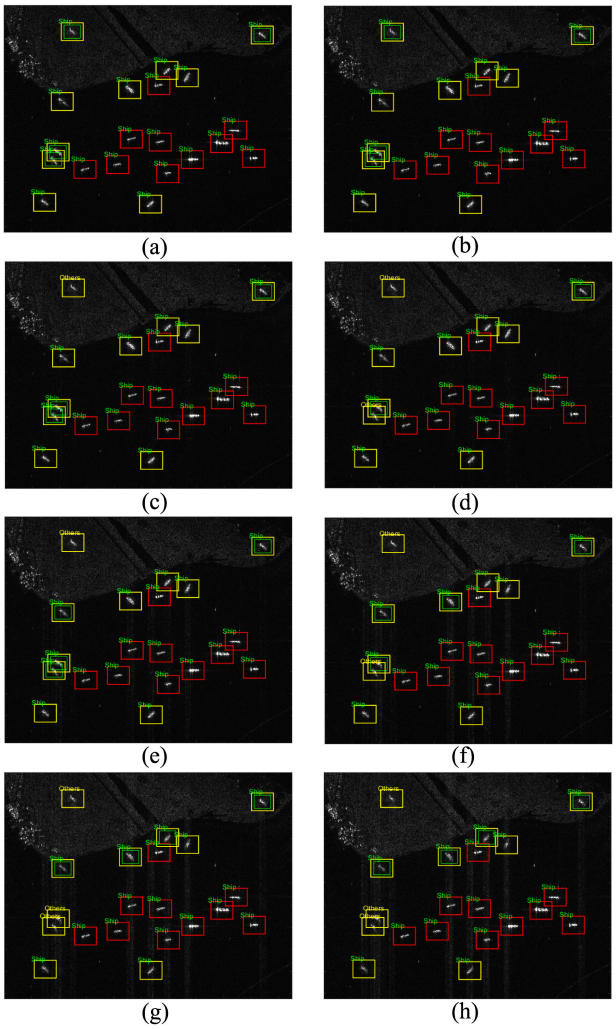

Fig. 11. Effect evaluation of repeater-jamming-based false ship targets on SAR images with closest slant range measurement errors being (a) 0, (b) 0.5%, (c) 2.5%, (d) 5%, (e) 10%, (f) 15%, (g) 20%, and (h) 25%, respectively.

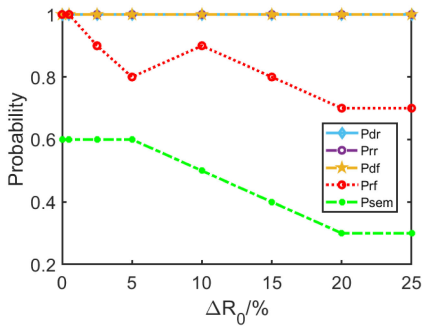

Fig. 12. Probability-related evaluation results versus different closest slant range measurement errors.

image-quality-related metrics are concluded in Table VI. The subscript jam in the evaluation tables means the image quality measured after being jammed.

For a lower closest slant range measurement error, more targets are successfully detected and recognized. This shows that the false targets have a similar response to the real ones and can

TABLE VI
IMAGE-QUALITY-RELATED METRICS WITH DIFFERENT CLOSEST SLANT RANGE MEASUREMENT ERRORS

ΔR_0	Metrics						
	H	ENL	H_{jam}	ENL_{jam}	d	ρ	$SSIM$
0	4.84	5.59	4.62	3.27	9707.79	0.894	0.898
0.5%	4.84	5.59	4.62	3.27	9716.63	0.893	0.897
2.5%	4.84	5.59	4.61	3.76	9534.44	0.899	0.894
5%	4.84	5.59	4.61	3.77	9564.80	0.898	0.892
10%	4.84	5.59	4.69	4.15	9314.61	0.904	0.873
15%	4.84	5.59	4.86	4.80	9090.37	0.912	0.865
20%	4.84	5.59	5.00	5.56	8944.74	0.918	0.854
25%	4.84	5.59	5.04	5.83	8859.52	0.922	0.845

confuse the SAR image interpretation. Note the two false targets at the top of Fig. 11(b); due to their wrong position, they are unfortunately generated on land resulting in semantic error. As a result, they are distinguished out by the aforementioned JSd with the background template of waters scene. Marked by the green box, they consequently fail to jam SAR ultimately. Meanwhile, there are two false targets, which, although reasonably generated on the sea area, are marked as semantic errors. The reason lies in that the two ships are so close to each other, which is unusual in practice in terms of safety concerns. Besides, caused by larger measurement error, more serious defocus of false targets can change the statistical properties of the background around them. Taking false targets as the centers, the white vertical lines caused by defocus extend to both ends along azimuth, which is clearly shown in Fig. 11(h). Consequently, false targets are more likely to be considered as semantically incorrect; such a phenomenon becomes apparent when the error reaches 5%, as visually illustrated in Fig. 12. In contrast, traditional metrics, which only measure the change of image quality, are impossible to reveal such details. Through the evaluation, we can reveal the facts that the generated high-fidelity false targets not only change the amplitude characters of the SAR image, but also have similar behavior in detection and recognition compared to the real ones. Therefore, they show a high degree of VC and, indeed, have an impact on SAR image interpretation. Additionally, benefiting from the consideration of semantic rationality, the unreasonable location can further be revealed, thus fully evaluating the effect of deceptive jamming on the SAR image. Overall speaking, considerations of multiple levels of vision have ensured rational and quantitative description of deception in our evaluation framework, which are further confirmed by the evaluation behaviors under different closest slant range measurement errors.

2) Velocity Measurement Errors: To analyze the influence of different velocity measurement errors on the deceptive jamming evaluation flow, varying velocity deviations are added when generating the false targets. Relative to the real velocity of a moving SAR platform, the measurement error ratios are 0, 0.5%, 1%, 3%, 5%, 7%, 10%, and 20%, respectively. Taking the origin SAR image with no jamming as the reference, the proposed evaluation framework is experimented. Through a series of simulations, false targets with different velocity errors are obtained, and the corresponding evaluation results are illustrated in Fig. 13.

As shown in Fig. 13, the increasing measurement error of velocity is directly related to the gradually worse imaging quality

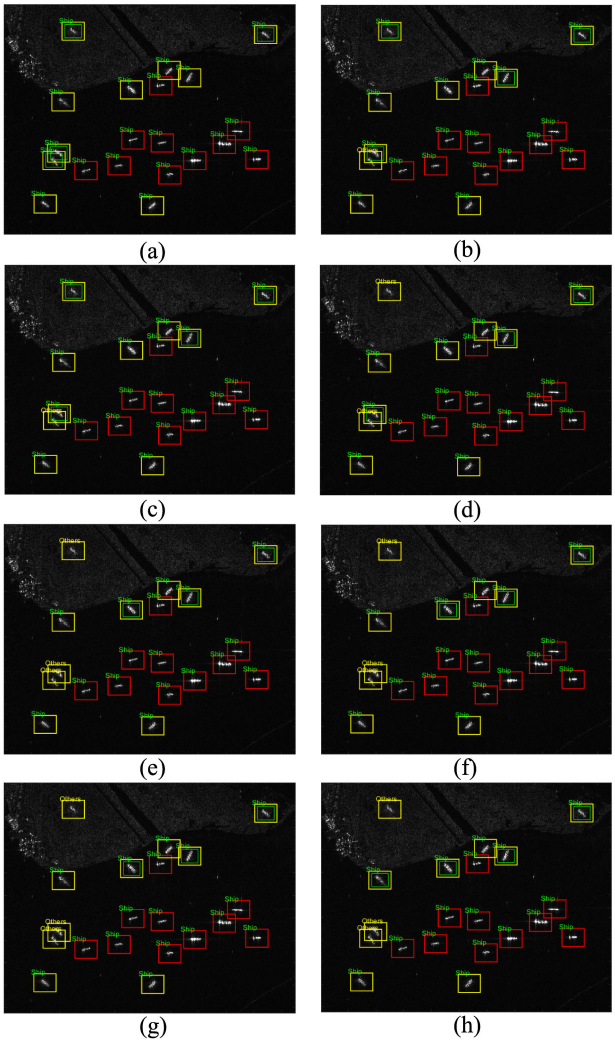

Fig. 13. Effect evaluation of repeater-jamming-based false ship targets on SAR images with velocity measurement errors being (a) 0, (b) 0.5%, (c) 1%, (d) 3%, (e) 5%, (f) 7%, (g) 10%, and (h) 20%, respectively.

of the false targets, although it is obviously less than the closest slant range measurement error. Recall that the motion velocity directly affects both the Doppler centroid frequency and the Doppler FM rate of the compensated signal, as derived in (6). Accordingly, a larger velocity measurement error implies a more serious stretching and defocus along azimuth, which damages the feature extracted from false targets. For expression, the labels in the images of evaluation results are the same as mentioned earlier.

As shown in Fig. 13, when the velocity measurement error exists, false targets are defocused around their original location and stretch along azimuth simultaneously. Such a phenomenon only affects a small fraction of the SAR image, thus causing limited degradation on the overall image quality. As listed in Table VII, traditional metrics all vary very little under different error circumstances. They cannot reflect the confusion of deceptive jamming and are, thus, impractical and ineffective. Fortunately, the proposed evaluation method based on VC can

TABLE VII
IMAGE-QUALITY-RELATED METRICS WITH DIFFERENT VELOCITY MEASUREMENT ERROR

ΔV	Metrics						
	H	ENL	H_{jam}	ENL_{jam}	d	ρ	$SSIM$
0	4.84	5.59	4.62	3.26	9707.79	0.8936	0.8976
0.5%	4.84	5.59	4.58	3.58	9647.80	0.8964	0.9075
1%	4.84	5.59	4.58	3.58	9652.99	0.8963	0.9075
3%	4.84	5.59	4.58	3.57	9680.07	0.8957	0.9074
5%	4.84	5.59	4.58	3.56	9700.72	0.8953	0.9074
7%	4.84	5.59	4.58	3.55	9714.76	0.8950	0.9074
10%	4.84	5.59	4.58	3.54	9750.92	0.8943	0.9073
20%	4.84	5.59	4.59	3.52	9806.15	0.8932	0.9067

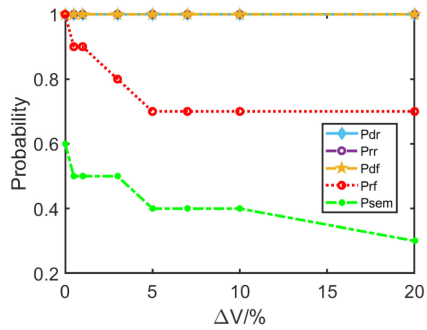

Fig. 14. Probability-related evaluation results versus different velocity measurement errors.

evaluate this phenomenon much more accurately and appropriately. The corresponding performance declines of recognition and semantic accuracy of false targets are keenly depicted, as illustrated in Fig. 14. When there is no velocity error, high-fidelity false targets can obtain the metrics of P_{rf} and P_{sem} with larger value, which means they appear a high property of VC and are, thus, much deceptive. With the increasing measurement error, false targets gradually fail to be recognized correctly, let along the semantic rationality. Correspondingly, the deception is weakened and evaluation metrics get worse. Note that even if there is a larger measurement error, the major parts of false targets are still relatively concentrated, so they can still be detected. In this case, low-level vision alone is not effective in evaluating the deception, while visual considerations of higher levels are more competent. Besides, from the evaluation results illustrated in Fig. 14, one can see that when the velocity measurement error reaches 5%, there will be more obvious impact on the deception changes of false targets. Therefore, compared with the traditional image-quality-based evaluation methods, the proposed evaluation framework, synthetically considering three levels of vision, has better accuracy and logicality.

C. False-Image-Jamming-Based Evaluation Experiments

In practice, SAR may be affected by different jamming with varying generation mechanisms. Here, the false targets generated according to the principle of false image jamming are considered. To evaluate the deceptive influence, several experiments are conducted. Note that during the implementation of false image jamming, more prior information about SAR or more sufficient and accurate parameters is considered to

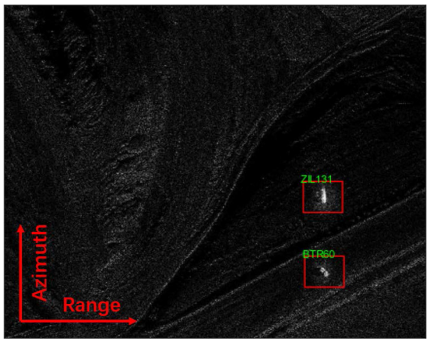

Fig. 15. Jamming-free SAR image that acts as a reference.

be available, which is guaranteed by outstanding intelligence acquisition or fine reconnaissance. Even so, the varying SNRs, as well as possible multiresolution modes of adversary SAR during jamming, can still affect the jamming results. Therefore, varying SNRs and resolutions are considered as nonideal factors for evaluation here.

The evaluation process is similar to the previous jamming case. The image pair to be processed first go through the TSTP-CFAR-based detection flow, and then, recognition with the especially designed CNN is carried out for the multiclass issue. Additionally, JSd-based semantic accuracy is considered to analyze the logic correctness of false targets with the corresponding background. Finally, the evaluation framework ends with metric calculation. The detection and recognition results of the original jamming-free SAR image are shown in Fig. 15 with the parameters listed in Table I. Two tanks, respectively, named ZIL131 and BTR60, are successfully detected and recognized as the reference for subsequent evaluations. Note that the tank target templates are of multiple categories, and the adopted CNN is trained under a multiclass classification situation. Therefore, a multiclass recognition is considered here, and the specific target category will be given in the recognition results. Besides, traditional metrics are also considered for comparison. Similarly, azimuth is on the vertical direction, whereas range lies along the horizontal one.

1) Varying SNRs: For evaluation, five false targets are generated and integrated into the origin SAR image via the deceptive mechanism of false image jamming; the related parameters are shown in Table I. Note that 2-D windowing is considered when processing the templates of false targets, thereby the edges of false targets are not obtrusive compared to the surrounding environment and, thus, well integrated into the SAR image. Considering the influence of varying SNRs on deceptive jamming effect evaluation, noise power is properly adjusted to obtain seven levels of SNR ranging from 10 to -20 dB at the step of 5 dB. The evaluation framework is experimented with the origin jamming-free SAR image in Fig. 15 acting as the reference.

As can be seen from Fig. 16, the gradually increasing noise makes the SAR image blurred correspondingly, including the real targets and false targets. For result representation of detection and recognition, the meanings of boxes and characters with different colors in the images are the same as those mentioned earlier. The semantic accuracy is likewise considered for the

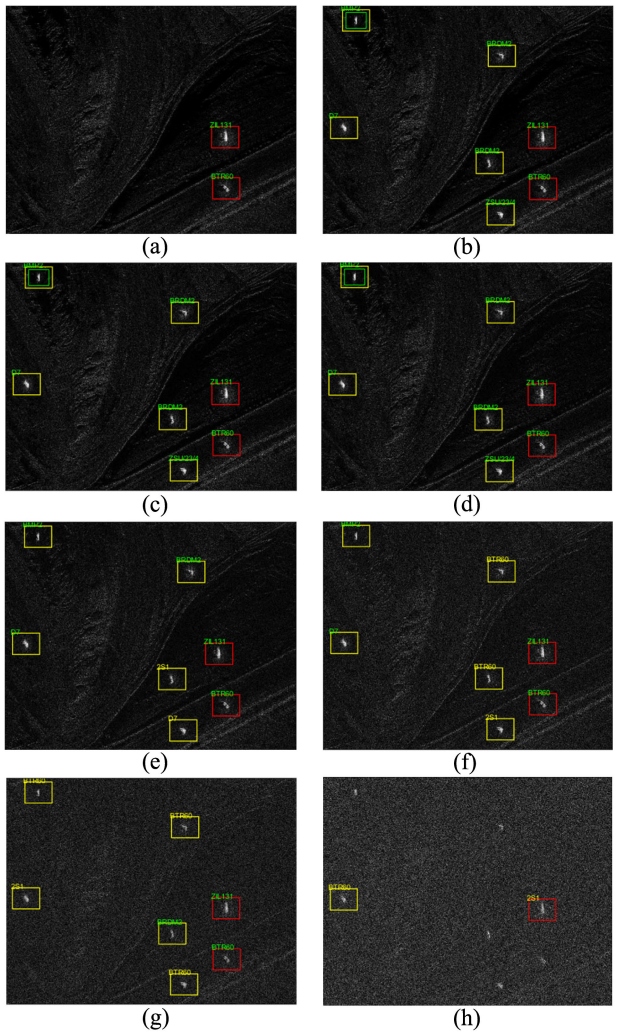

Fig. 16. Effect evaluation of false-image-jamming-based false tank targets on SAR images with varying SNRs. (a) Reference. Evaluation results with different SNRs are (b) 10 dB, (c) 5 dB, (d) 0 dB, (e) -5 dB, (f) -10 dB, (g) -15 dB, and (h) -20 dB.

TABLE VIII
IMAGE-QUALITY-RELATED METRICS WITH VARYING SNRS

SNR	Metrics						
	H	ENL	H_{jam}	ENL_{jam}	d	ρ	$SSIM$
10dB	5.48	25.05	5.49	14.95	6001.76	0.954	0.945
5dB	5.48	25.05	5.49	15.72	6422.86	0.949	0.909
0dB	5.48	25.05	5.46	17.91	12515.25	0.802	0.472
-5dB	5.48	25.05	5.48	29.98	13071.07	0.907	0.456
-10dB	5.48	25.05	5.76	54.42	13949.83	0.847	0.449
-15dB	5.48	25.05	6.06	218.63	20809.73	0.769	0.239
-20dB	5.48	25.05	6.59	1428.84	35233.81	0.694	0.059

successfully detected and recognized false targets. For instance, a tank cannot appear on a lake or in a steep slope. False targets with unnatural background positions will be framed in green rectangles. As shown in Fig. 16, both real targets and false targets are affected when being detected and recognized due to the gradually worse SNR. And the deteriorated image quality can be obtained in Table VIII. In addition, Fig. 17 clearly shows the trend of detection and recognition performance against

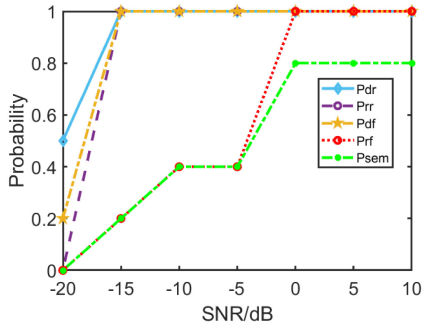

Fig. 17. Probability-related evaluation results versus varying SNRs.

varying SNRs. For higher SNRs, false targets show the similar response to the processing flow as real ones do, which indicates their succeeding in confusing the adversary due to high VC. As the SNR goes down to −5 dB here, the features of false targets are damaged by noise, which inevitably affects the recognition performance and also causes a decline in deception. Besides, note the false target in the upper left corner of Fig. 16(b); it is flagged by the green box because of its semantic irrationality. This region was originally a shaded area due to layover caused by a steep slope, which is not a common place for tanks. However, when the SNR decreases to a certain extent like −5 dB here, the dark area is filled with noise, which results in the changes of statistical properties of the corresponding background. The false target that is originally with incorrect semantics gradually gets rid of suspicion.

Through the analysis of evaluation results, it can be seen that the effects of false targets on SAR images are mainly concentrated in the deceptive features of deceiving SAR interpretation, while the specific performance can be affected by different levels of SNRs. Meanwhile, the adopted semantic accuracy is proved to have the ability to reveal the logical rationality of the false targets' positioning. Having considered more practical factors and analyzed in the novel view of VC, the evaluation framework is, thus, more efficient and reasonable. Besides, the evaluation results obtained under different SNRs can more sufficiently reveal the evaluation performance of expounding the confusion of deceptive jamming.

2) Varying Resolutions: False targets are generated according to the obtained reconnaissance information; simultaneously, the corresponding target templates are designed and act as the input of the adopted CNN for training. Nevertheless, there is usually a possibility that the SAR system, which serves as the object for jamming, can operate in multiple resolution modes. For the variable resolutions, target templates and recognition network are difficult to be generated in real time. Therefore, effect evaluation under different resolutions based on the recognition configuration at a specific resolution should be considered. Accordingly, behavior analysis of the proposed evaluation method under different resolutions is carried out here. By changing the antenna size along azimuth, the azimuth resolutions are set as 0.8, 1, and 1.2 m, respectively, and the range resolution is proportionally scaled accordingly. The result at an azimuth resolution of 0.8 m in Fig. 15 is again used as a reference

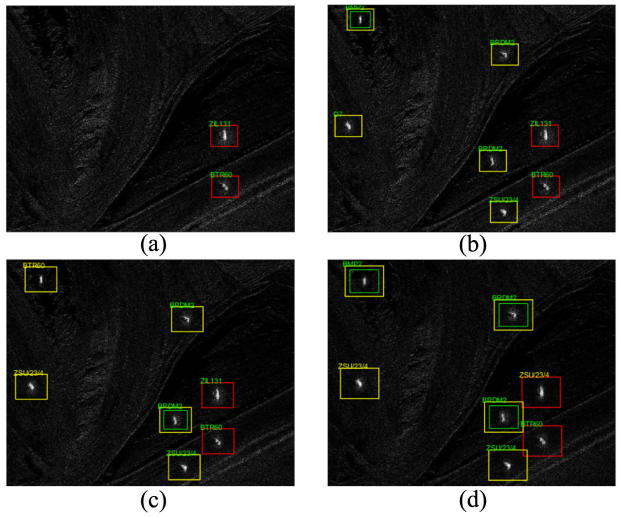

Fig. 18. Effect evaluation of false-image-jamming-based false tank targets on SAR images with varying resolutions. (a) Reference. Evaluation results with different resolutions are (b) 0.8 m, (c) 1 m, and (d) 1.2 m.

for evaluation. Besides, the corresponding processing results are shown in Fig. 18, which reveals the variation trend versus varying resolutions.

As illustrated in Fig. 18, as the resolution gets worse, detailed textures of the SAR imaging result gradually deteriorate. The whole image, including all the targets, gets blurry; meanwhile, the number of imaging scatterers becomes fewer. Due to the varying resolution, both the scattering characteristics of targets and backgrounds are correspondingly changed. Therefore, the recognition features of targets show some differences, which can reduce the probability of being successfully recognized and result in a worse VC. Fig. 18(b) shows the evaluation result at an azimuth resolution of 0.8 m, which is the same resolution value as that used for template generation. Consequently, the targets are correctly recognized because of the matched resolution, and deception of false targets is fully performed due to their corresponding high VC. As the resolution gradually moves away from the reference one, although false targets can be accurately detected, there comes the instability in recognition and semantic analysis results. Such behaviors can be keenly described by the VC-related metrics P_{rf} and P_{sem} shown in Table IX. Besides, for the image-quality-related metrics, most of them are insensitive to the varying resolution and, thus, not qualified for evaluation of deceptive jamming. It can be seen from the evaluation results that only when the resolution is matched, the expected deceptive performance can be achieved. In addition, these evaluation results can, in turn, remind the jammer to pay attention to the jamming generation under multiple resolution situations.

With above experiments, it is convinced that the proposed VC-based evaluation framework has a more reasonable and finely detailed description of the confusion of false targets compared with the traditional evaluation methods. Meanwhile, the proposed evaluation framework can be effectively implemented even under different deceptive jamming with various nonideal factors. Moreover, the effective evaluation results can not only help the defender to make strategic adjustment in time, but also

TABLE IX
METRICS WITH VARYING RESOLUTIONS

Resolution	Metrics											
	H	ENL	H_{jam}	ENL_{jam}	d	ρ	$SSIM$	P_{dr}	P_{rr}	P_{df}	P_{rf}	P_{sem}
0.8m	5.477	25.050	5.49	14.59	5582.12	0.960	0.978	1	1	1	1	0.8
1m	5.253	18.469	5.25	9.78	4758.13	0.945	0.971	1	1	1	0.6	0.4
1.2m	5.028	14.230	5.07	6.87	3995.67	0.929	0.979	1	0.5	1	0.8	0.2

guide the attacker to improve the undesirable deception effects caused by various undesirable factors.

V. CONCLUSION

In this article, the evaluation framework of deceptive jamming effect on SAR is proposed via fusion of multilevel visions, which is demonstrated superior to the traditional metrics that only focus on the description of the suppression effect. The well-designed detection and recognition flows ensure the satisfying implementation of effect evaluation. Moreover, the influence of deceptive jamming with several nonideal issues is considered. By comparing the evaluation results obtained by traditional metrics with that by the proposed VC-related metrics, we can draw the conclusion that the latter can more accurately and logically reveal the influence of deceptive confusion on SAR image interpretation. The reason lies in our sufficient considerations on high fidelity. Besides, the proposed semantic accuracy, along with its concrete calculation, plays an outstanding role in describing the location rationality of false targets. Both qualitative and quantitative experiments demonstrate the significance and practicality of the proposed evaluation framework. In addition, future work will be focused on increasing the template diversity of the target and background and improving the framework to adapt to more complex imaging scenes.

REFERENCES

[1] E. Makhoul, A. Broquetas, J. R. Rodon, Y. Zhan, and F. Ceba, "A performance evaluation of SAR-GMTI missions for maritime applications," *IEEE Trans. Geosci. Remote Sens.*, vol. 53, no. 5, pp. 2496–2509, May 2015.

[2] S.-W. Chen, X.-S. Wang, and S.-P. Xiao, "Urban damage level mapping based on co-polarization coherence pattern using multitemporal polarimetric SAR data," *IEEE J. Sel. Topics Appl. Earth Observ. Remote Sens.*, vol. 11, no. 8, pp. 2657–2667, Aug. 2018.

[3] S. Samsonov, "Topographic correction for ALOS PALSAR interferometry," *IEEE Trans. Geosci. Remote Sens.*, vol. 48, no. 7, pp. 3020–3027, Jul. 2010.

[4] A. Moreira, P. Prats-Iraola, M. Younis, G. Krieger, I. Hajnsek, and K. P. Papathanassiou, "A tutorial on synthetic aperture radar," *IEEE Geosci. Remote Sens. Mag.*, vol. 1, no. 1, pp. 6–43, Mar. 2013.

[5] S. Chen, Y. Yuan, S. Zhang, H. Zhao, and Y. Chen, "A new imaging algorithm for forward-looking missile-borne bistatic SAR," *IEEE J. Sel. Topics Appl. Earth Observ. Remote Sens.*, vol. 9, no. 4, pp. 1543–1552, Apr. 2016.

[6] F. Zhou, B. Zhao, M. Tao, X. Bai, B. Chen, and G. Sun, "A large scene deceptive jamming method for space-borne SAR," *IEEE Trans. Geosci. Remote Sens.*, vol. 51, no. 8, pp. 4486–4495, Aug. 2013.

[7] F. Zhou, T. Tian, B. Zhao, X. Bai, and W. Fan, "Deception against near-field synthetic aperture radar using networked jammers," *IEEE Trans. Aerosp. Electron. Syst.*, vol. 55, no. 6, pp. 3365–3377, Dec. 2019.

[8] B. Zhao, L. Huang, F. Zhou, and J. Zhang, "Performance improvement of deception jamming against SAR based on minimum condition number," *IEEE J. Sel. Topics Appl. Earth Observ. Remote Sens.*, vol. 10, no. 3, pp. 1039–1055, Mar. 2017.

[9] B. Zhao, F. Zhou, and Z. Bao, "Deception jamming for squint SAR based on multiple receivers," *IEEE J. Sel. Topics Appl. Earth Observ. Remote Sens.*, vol. 8, no. 8, pp. 3988–3998, Aug. 2015.

[10] Z. Tang, Y. Deng, H. Zheng, and R. Wang, "High-fidelity SAR intermittent sampling deceptive jamming suppression using azimuth phase coding," *IEEE Geosci. Remote Sens. Lett.*, vol. 18, no. 3, pp. 489–493, Mar. 2021.

[11] W. Zhu, X. Jia, and X. Pan, "Cross-entropy for effect evaluation of jamming to synthetic aperture radar," in *Proc. IET Int. Conf. Wireless, Mobile, Multimedia Netw.*, Nov. 2006, pp. 1–4.

[12] X. Li and J. Zhen, "Information theory-based amendments of SAR jamming effect evaluation," in *Proc. 6th Int. Conf. Internet Comput. Sci. Eng.*, Apr. 2012, pp. 159–162.

[13] W. Zhu, Y. Zhou, and C. Li, "A new index for effectiveness measure of jamming to synthetic aperture radar," in *Proc. 8th Int. Conf. Signal Process.*, Nov. 2006, pp. 1–4.

[14] M. A. Ammar, H. A. Hassan, M. S. Abdel-Latif, and S. A. Elgamel, "Performance evaluation of SAR in presence of multiplicative noise jamming," in *Proc. 34th Nat. Radio Sci. Conf.*, Mar. 2017, pp. 213–220.

[15] X. F. Wu, D. H. Dai, and X. S. Wang, "Study on SAR jamming measures," in *Proc. IET Int. Conf. Radar Syst.*, Oct. 2007, pp. 1–5.

[16] G. X. Wang, S. R. Peng, J. J. Sun, and H. He, "Effect evaluation for SAR suppression jamming based on edge strength image," in *Proc. IET Int. Radar Conf.*, Oct. 2015, pp. 1–4.

[17] X. Wu, D. Dai, X. Wang, and H. Lu, "Evaluation of SAR jamming performance," in *Proc. Int. Symp. Microw., Antenna, Propag., EMC Technol. Wireless Commun.*, Aug. 2007, pp. 1476–1480.

[18] Z. Wang, A. C. Bovik, H. R. Sheikh, and E. P. Simoncelli, "Image quality assessment: From error visibility to structural similarity," *IEEE Trans. Image Process.*, vol. 13, no. 4, pp. 600–612, Apr. 2004.

[19] Z. Liu and K. Xu, "The effectiveness index of SAR jamming based on information loss of images," *Acta Electron. Sinica*, vol. 35, no. 6, pp. 1042–1045, 2007.

[20] J. Shuhong, L. Mingzhu, and D. Weisheng, "Evaluation of jamming effect on SAR based on textural feature," in *Proc. Int. Conf. Inf. Commun. Manage.*, Dec. 2012, pp. 13–18.

[21] Y. Lee, J. Park, W. Shin, K. Lee, and H. Kang, "A study on jamming performance evaluation of noise and deception jammer against SAR satellite," in *Proc. 3rd Int. Asia-Pacific Conf. Synthetic Aperture Radar*, Sep. 2011, pp. 1–3.

[22] B. Zhonggan, D. Xingsong, Z. Lei, and H. Letian, "Centroid-track based method for SAR jamming effect evaluation," in *Proc. 13th IEEE Int. Conf. Electron. Meas. Instrum.*, Oct. 2017, pp. 406–410.

[23] J. J. Shi, D. P. Bi, and L. Xue, "Novel evaluation method of jamming effect on ISAR based on target detection," in *Proc. 2nd Asian-Pacific Conf. Synth. Aperture Radar*, 2009, pp. 892–895.

[24] T.-Y. Shen, J.-J. Ding, Y. Ding, and J.-G. Shi, "A method of detection performance modeling in jamming condition based on radar network system," in *Proc. IEEE CIE Int. Conf. Radar*, vol. 2, Oct. 2011, pp. 1366–1369.

[25] T. Tian *et al.*, "Performance evaluation of deception against synthetic aperture radar based on multifeature fusion," *IEEE J. Sel. Topics Appl. Earth Observ. Remote Sens.*, vol. 14, 2021, pp. 103–115.

[26] J. Ai, X. Yang, J. Song, Z. Dong, L. Jia, and F. Zhou, "An adaptively truncated clutter-statistics-based two-parameter CFAR detector in SAR imagery," *IEEE J. Ocean. Eng.*, vol. 43, no. 1, pp. 267–279, Jan. 2018.

[27] K. El-Darymli, P. Mcguire, D. Power, and C. Moloney, "Target detection in synthetic aperture radar imagery: A state-of-the-art survey," *J. Appl. Remote Sens.*, vol. 7, no. 1, pp. 1–35, May 2013.

[28] Z. Cui, H. Quan, Z. Cao, S. Xu, C. Ding, and J. Wu, "SAR target CFAR detection via GPU parallel operation," *IEEE J. Sel. Topics Appl. Earth Observ. Remote Sens.*, vol. 11, no. 12, pp. 4884–4894, Dec. 2018.

[29] X. Xing, Z. Chen, H. Zou, and S. Zhou, "A fast algorithm based on two-stage CFAR for detecting ships in SAR images," in *Proc. 2nd Asian-Pacific Conf. Synth. Aperture Radar*, Oct. 2009, pp. 506–509.

[30] S. Chen, H. Wang, F. Xu, and Y.-Q. Jin, "Target classification using the deep convolutional networks for SAR images," *IEEE Trans. Geosci. Remote Sens.*, vol. 54, no. 8, pp. 4806–4817, Aug. 2016.
[31] J. H. Cho and C. G. Park, "Multiple feature aggregation using convolutional neural networks for SAR image-based automatic target recognition," *IEEE Geosci. Remote Sens. Lett.*, vol. 15, no. 12, pp. 1882–1886, Dec. 2018.
[32] S. Deng, L. Du, C. Li, J. Ding, and H. Liu, "SAR automatic target recognition based on Euclidean distance restricted autoencoder," *IEEE J. Sel. Topics Appl. Earth Observ. Remote Sens.*, vol. 10, no. 7, pp. 3323–3333, Jul. 2017.
[33] Y. Duan *et al.*, "Adaptive hierarchical multinomial latent model with hybrid kernel function for SAR image semantic segmentation," *IEEE Trans. Geosci. Remote Sens.*, vol. 56, no. 10, pp. 5997–6015, Oct. 2018.
[34] H. Bi, L. Xu, X. Cao, Y. Xue, and Z. Xu, "Polarimetric SAR image semantic segmentation with 3D discrete wavelet transform and Markov random field," *IEEE Trans. Image Process.*, vol. 29, pp. 6601–6614, Jun. 2020.
[35] W. Yang, H. Song, X. Huang, X. Xu, and M. Liao, "Change detection in high-resolution SAR images based on Jensen–Shannon divergence and hierarchical Markov model," *IEEE J. Sel. Topics Appl. Earth Observ. Remote Sens.*, vol. 7, no. 8, pp. 3318–3327, Aug. 2014.
[36] J. Lin, "Divergence measures based on the Shannon entropy," *IEEE Trans. Inf. Theory*, vol. 37, no. 1, pp. 145–151, Jan. 1991.
[37] S. Ioffe and C. Szegedy, "Batch normalization: Accelerating deep network training by reducing internal covariate shift," in *Proc. 32nd Int. Conf. Mach. Learn.*, Mar. 2015, pp. 448–456.
[38] K. Fu, F.-Z. Dou, H.-C. Li, W.-H. Diao, X. Sun, and G.-L. Xu, "Aircraft recognition in SAR images based on scattering structure feature and template matching," *IEEE J. Sel. Topics Appl. Earth Observ. Remote Sens.*, vol. 11, no. 11, pp. 4206–4217, Nov. 2018.
[39] A. Saini, A. Agarwal, and D. Singh, "Feature-based template matching for joggled fishplate detection in railroad track with drone images," in *Proc. IEEE Int. Geosci. Remote Sens. Symp.*, Oct. 2020, pp. 2237–2240.
[40] X. Lin, P. Liu, and G. Xue, "Fast generation of SAR deceptive jamming signal based on inverse range Doppler algorithm," in *Proc. IET Int. Radar Conf.*, Apr. 2013, pp. 1–4.
[41] I. G. Cumming and F. H. Wong, *Digital Processing of Synthetic Aperture Radar Data: Algorithms and Implementation*. Norwood, MA, USA: Artech House, 2005.
[42] P. Xia and T. Tang, "Watershed image segmentation based on nonlinear combination morphology filter," in *Proc. 4th Int. Congr. Image Signal Process.*, vol. 4, 2011, pp. 2026–2029.
[43] A. Yang, "Research on image filtering method to combine mathematics morphology with adaptive median filter," in *Proc. 9th Int. Conf. Opt. Commun. Netw.*, 2010, pp. 55–59.
[44] M. Weng and M. He, "Image feature detection and matching based on SUSAN method," in *Proc. 1st Int. Conf. Innovative Comput. Inf. Control*, vol. 1, 2006, pp. 322–325.
[45] H. Yang, C. Huang, F. Wang, K. Song, and Z. Yin, "Robust semantic template matching using a superpixel region binary descriptor," *IEEE Trans. Image Process.*, vol. 28, no. 6, pp. 3061–3074, Jun. 2019.
[46] K. Simonyan and A. Zisserman, "Very deep convolutional networks for large-scale image recognition," in *Proc. 3rd Int. Conf. Learn. Represent.*, May 2015, pp. 1–14.
[47] C. Szegedy, V. Vanhoucke, S. Ioffe, J. Shlens, and Z. Wojna, "Rethinking the inception architecture for computer vision," in *Proc. IEEE Conf. Comput. Vis. Pattern Recognit.*, Jun. 2016, pp. 2818–2826.
[48] D. P. Kingma and J. L. Ba, "Adam: A method for stochastic optimization," in *Proc. Int. Conf. Learn. Represent.*, Dec. 2014, pp. 1–15.

Zhouyang Tang was born in Hunan, China, in 1995. He received the B.S. degree in space science and technology from Xidian University, Xi'an, China, in 2017. He is currently working toward the Ph.D. degree with the Department of Space Microwave Remote Sensing System, Aerospace Information Research Institute, Chinese Academy of Sciences, Beijing, China.

He is also with the University of Chinese Academy of Sciences, Beijing. His research interests include synthetic aperture radar (SAR) imaging, SAR countermeasure, and interference suppression.

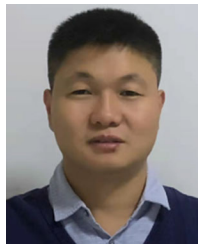

Chunrui Yu received the Ph.D. degree in signal processing from the National University of Defense Technology, Changsha, China, in 2012.

He is currently a Research Associate with the Beijing Institute of Tracking and Telecommunication Technology, Beijing, China. His research interests include synthetic aperture radar (SAR) system design, SAR jamming and antijamming, and space-time adaptive processing.

Yunkai Deng (Member, IEEE) received the M.S. degree in electrical engineering from the Beijing Institute of Technology, Beijing, China, in 1993.

In 1993, he joined the Institute of Electronics, Chinese Academy of Sciences (IECAS), Beijing, where he was involved in antenna design, microwave circuit design, and spaceborne/airborne synthetic aperture radar (SAR) technology. Since 1993, he has been a Research Fellow with the Department of Space Microwave Remote Sensing System, IECAS. He has been the Leader of several spaceborne/airborne SAR programs and developed some key technologies of spaceborne/airborne SAR. Since 2012, he has been a Principal Investigator with the Helmholtz–Chinese Academy of Sciences Joint Research Group, Beijing, concerning Spaceborne Microwave Remote Sensing for Prevention and Forensic Analysis of Natural Hazards and Extreme Events. He is currently a Research Scientist with the University of the Chinese Academy of Sciences, Beijing. He has authored or coauthored more than 100 peer-reviewed and well-known journal articles since 2002. His research interests include spaceborne/airborne SAR technology for advanced modes, multifunctional radar imaging, and microwave circuit design.

Mr. Deng is a member of the Scientific Board. He was a recipient of several prizes, including the First and Second Class Rewards of National Defense Science and Technology Progress in 2007, the First Class Reward of the National Scientific and Technological Progress in 2008, the achievements of the Outstanding Award of the Chinese Academy of Sciences in 2009, and the First Class Reward of Army Science and Technology Innovation in 2016, for his outstanding contribution in SAR field.

Tingzhu Fang was born in Anhui, China, in 1996. He received the B.S. degree in electronical information science and technology from Central South University, Changsha, China, in 2017. He is currently working toward the Ph.D. degree with the Department of Space Microwave Remote Sensing System, Aerospace Information Research Institute, Chinese Academy of Sciences, Beijing, China.

He is also with the University of Chinese Academy of Sciences, Beijing. His research interests include synthetic aperture radar imaging and signal processing.

Huifang Zheng received the B.S. degree in electronic information engineering from Beijing Normal University, Beijing, China, in 2006, and the Ph.D. degree in communication and information systems from the University of Chinese Academy of Sciences, Beijing, in 2013.

She is currently working in the field of spaceborne synthetic aperture radar technology with the Aerospace Information Research Institute, Chinese Academy of Sciences, Beijing.